Soldering nanowires

DOI: 10.1002/smll.200500296

Reflow and Electrical Characteristics of Nanoscale Solder**

*Zhiyong Gu, Hongke Ye, Diana Smirnova, David Small, and David H. Gracias**

Solders or metallic alloys are used extensively in a wide range of electronic systems, including surface-mount circuit boards and device packages for integrated circuits (ICs),[1] to form conductive joints between electronic components. In existing devices, the size of solder joints range from millimeters in circuit boards to tens of micrometers in IC ball-grid-array[2] packages. In order to extend millimeter- and micrometer-scale electronic integration to the sub-micrometer and nanometer length scales, it is necessary to develop strategies to form electrically conductive joints between nanoparticles (isotropic or anisotropic) and between nanoparticles and substrates. At the present time, two strategies, either a) damascene integration[3] or b) molecular contacts,[4] are being utilized to form sub-micrometer scale interconnects. Damascene integration, which involves the photolithographic processes of patterning, etching, and deposition of metal, is used in copper interconnect layers in ICs. However, damascene integration is an inherently two-dimensional, layer-by-layer methodology that requires extensive processing steps. Moreover, it is prohibitively difficult to form electrical contacts between large numbers of nanoparticles using damascene integration. Although it is possible to form molecular electrical contacts between nanoparticles using self-assembly, organic molecules do not conduct electricity as well as metals and cannot survive high-temperature processing. Metallic solder allows components to be attached together in an easy and inexpensive manner. Moreover, solder joints are not sensitive to local roughness of components as solder forms a liquid during reflow. However, it is not clear if conventional solder will remain functional at the sub-micrometer and nanometer length scales, where the ratio of surface area to volume increases significantly. Solder degradation mechanisms, including oxidation, diffusion, and intermetallic formation, that do not significantly impact solder performance at the millimeter-to-10-μm length scales can render solder joints non-conductive at the sub-micrometer length scale.

There are very limited experiments investigating the use of metallic solder in sub-micrometer-scale applications. In one study, 100 nm of a single-component solder, indium (In), was evaporated on a substrate, and, upon heating the substrate, solder spheres with sizes as small as 5 nm were observed.[5] Although this experiment demonstrated that reflow might be possible on the nanoscale, the question of the functionality of solder to form an electrically conductive joint at sub-micrometer and nanometer length scales remained unanswered. In another study, a soldering technique for carbon nanotubes was carried out in a scanning electron microscope using amorphous carbon, which graphitizes under the electron-beam irradiation to form an electrical contact.[6] In a previous study, we demonstrated electrical bonding of nanoparticles to microscale solder pads patterned on substrates using solder reflow.[7]

In this communication, we demonstrate that nanoscale solder can be electrodeposited on rod-shaped metallic particles (also known as wires) grown in nanoporous membranes and that solder on these wires (diameter range of 30 to 200 nm) can be reflowed upon heating. In our experiments, the wires contained segments that optimized wetting of solder while limiting intermetallic diffusion. The nanoscale solder reflow was carried out in a home-built tube furnace where extreme care was taken to minimize oxidation of the joints. We were also able to fuse nanowires with each other using solder. The resistance of the fused wires was measured, and we observed electrical resistances that were consistent with a low-resistance ohmic solder joint.

We used the strategy of Martin[8] and Mallouk[9] to electrodeposit nanowires in porous membranes (templates) with a nominal pore size ranging from 30 to 200 nm (Figure 1A). We experimented with several different multicomponent

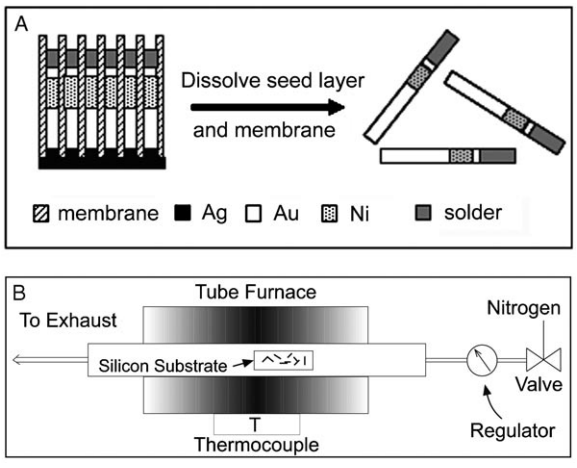

Figure 1. A) Schematic of the strategy used to fabricate nanowires using electrodeposition in a nanoporous membrane. B) Schematic diagram of the tube-furnace setup used to investigate solder reflow and joint formation.

[*] Dr. Z. Gu, Dr. H. Ye, D. Smirnova, D. Small, Prof. D. H. Gracias
Department of Chemical and Biomolecular Engineering
Johns Hopkins University
Baltimore, MD 21218 (USA)
Fax: (+1) 410-516-5510
E-mail: dgracias@jhu.edu
Prof. D. H. Gracias
Department of Chemistry
Johns Hopkins University, Baltimore, MD 21218 (USA)

[**] The donors of the American Chemical Society Petroleum Research Fund are acknowledged for partial support of this research. This research was supported in part by a National Science Foundation (NSF-DMII) CAREER Award. The authors acknowledge the assistance of Dr. Kenneth Livi in TEM measurements and analysis.

wires containing gold (Au), nickel (Ni), copper (Cu), silver (Ag), tin–lead solder (Sn/Pb, 60:40), Sn solder, and In solder segments. The wires that facilitated reproducible reflow consisted of four segments Au–Ni–Au–solder (Sn/Pb or Sn or In). The longest segment of the wire was made of Au, as gold is relatively inert and a good conductor of electricity. The Au segment was followed by a Ni segment (Ni functions as a diffusion barrier that reduces diffusion of Au into Sn) and then by a very thin layer of Au (Au layer enhances wetting by easily dissolving in solder). Finally, the wire was capped with a solder segment. While we did observe reflow of the Sn/Pb solder (Sn/Pb solder has been the most commonly used solder in the microelectronics industry), we often observed phase separation of Sn and Pb on electrodeposition, and it was difficult to get homogeneous reflow. Moreover, Pb is being gradually phased out of the microelectronics industry due to toxicity and environmental concerns.[10,11] Therefore, we focused our experiments on model lead-free solders, metallic Sn (melting point, m.p., 232 °C) and In (m.p. 157 °C) solder. Sn and In are components of most lead-free solders that are being considered as a replacement for Sn/Pb solder. While we observed reflow of the In solder, the In segments were easily corroded. The Sn-based solder on the other hand reflowed reproducibly, wetted Au well, and had good corrosion resistance. Hence, we utilized Sn as a model solder for our investigations.

Any corrosion of solder segments was minimized during release of the wires from the alumina membrane by adding benzotriazole (BTA) to the wire suspensions. BTA forms self-assembled molecular layers on several metallic surfaces,[12] including solder, thereby protecting the surfaces from corrosion. While solder corrosion on the macroscale can be removed by dissolution (and the solder regenerated) prior to reflow, any corrosion in solder segments on the 100-nm size scale and below severely depletes the solder and greatly limits solder joint formation.

Solder reflow was carried out in a home-built tube-furnace setup (Figure 1B). The furnace was designed to minimize oxidation of the joints while providing a uniform ambient temperature. The wires to be reflowed were dispersed on a silicon (Si, coated with silicon dioxide, SiO_2) substrate and introduced into the furnace. We purged the furnace with a stream of N_2 gas before, during, and after reflow. We minimized the dwell times above the peak reflow temperature to reduce interdiffusion of metals.

The rationale for using Au–Ni–Au–Sn wires in our experiments is evident from the results shown in Figure 2. When Sn segments were directly in contact with Au (Figure 2A), we observed interdiffusion of Au and Sn even before reflow. This is consistent with published results, where rapid interdiffusion of Au and Sn was observed in thin films at room temperature.[13–15] On reflow of the Au–Sn wire (Figure 2B), the diffusion of Au into Sn was extensive, and the shape of the wire changed dramatically. When a Ni spacer layer was added between the Au and Sn segments (Au–Ni–Sn wires) (Figure 2C), no diffusion of Au into the Sn segment was observed before reflow. The interdiffusion of Au and Sn in Au–Ni–Sn wires during reflow also decreased substantially (Figure 2D). While Ni behaves as an effective diffusion barrier, it is not wet well by solder, hence the shape of reflowed Sn segments on Au–Ni–Sn wires appeared very irregular (Figure 2D). To enchance wetting of the solder on the Ni segment, we inserted a thin Au segment (100–200 nm) between the Ni and the Sn segments. Hence, the model wires used in the study consisted of Au–Ni–Au–Sn segments (Figure 3).

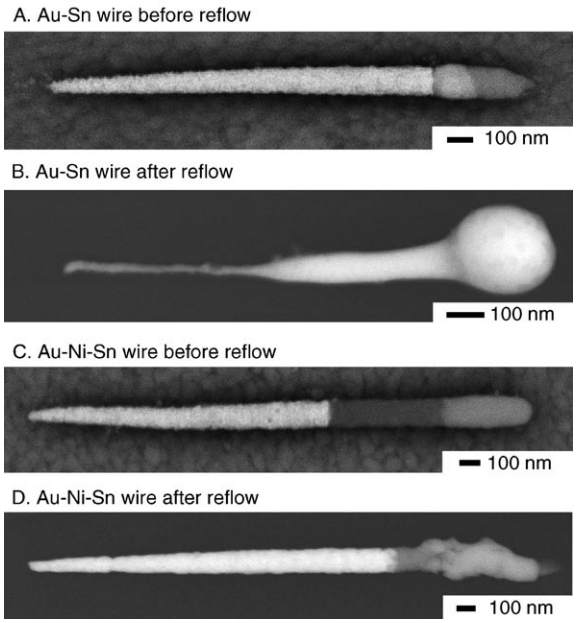

Figure 2. Scanning electron microscopy (SEM) images of nanowires (nominal diameter of 50 nm) with different compositions, before and after reflow. A) A typical Au–Sn nanowire (before reflow), B) Au–Sn nanowire (after reflow), C) Au–Ni–Sn nanowire (before reflow), and D) Au–Ni–Sn nanowire (after reflow). The contrast in backscatter SEM images is related to the atomic number of the species being imaged: hence Au (highest atomic number) appears the brightest, followed by Sn, and then Ni (lowest atomic number).

Shown in Figure 3 are 200-, 50-, and 30-nm diameter Au–Ni–Au–Sn wires before and after reflow. There was a dramatic change observed after reflow only at one end of the nanowire—a large bulge—consistent with the melting of solder at that end. We did control experiments using nanowires without Sn segments and observed no discernible change in the wires on heating.

Au–Ni–Au–Sn nanowires (Figure 4) deposited on a holey carbon copper grid were imaged using transmission electron microscopy (TEM) before and after reflow. Even before reflow we observed the presence of a segment containing both Au and Sn (Figure 4B, position d), which is consistent with the diffusion of Au into Sn, as observed in Figure 2A and discussed earlier. From EDS quantification analysis, the atomic-weight ratio of Au:Sn at position d in Figure 4 was approximately 1:0.8, indicating an AuSn-type intermetallic. Au is known to diffuse into Sn to form intermetallics—AuSn in the Au-rich regions and $AuSn_2$, $AuSn_4$ in the Sn-rich regions even at room temperature.[14,16] The interdiffusion of Au and Sn increases the wettability of the Sn solder on the wire on reflow but leads to a higher electrical resistance, although the difference is not very dramatic

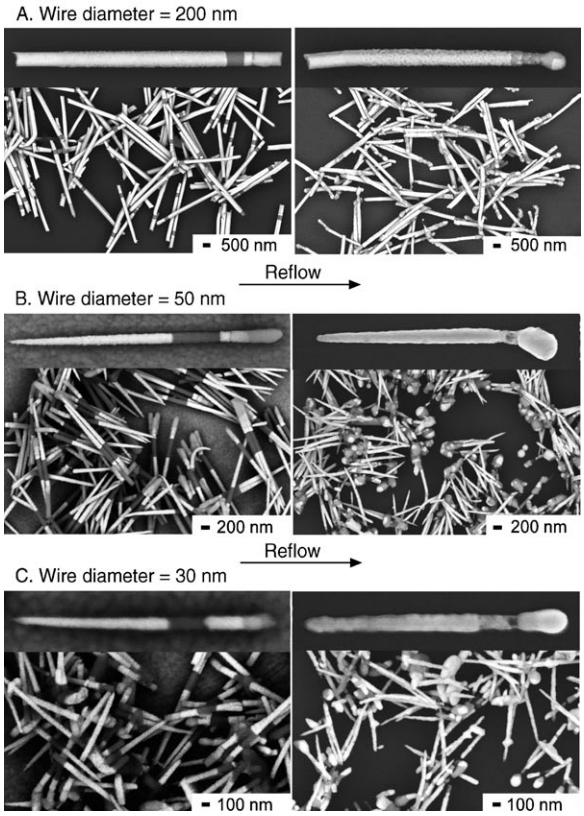

Figure 3. SEM images of Au–Ni–Au–Sn nanowires, of different diameters, before and after solder reflow. Each image shows a large number of wires and a zoomed image of a single wire. The nominal wire diameters are A) 200, B) 50, and C) 30 nm. There was a dramatic bulge observed at one end of the wire on reflow, which is consistent with the melting of Sn.

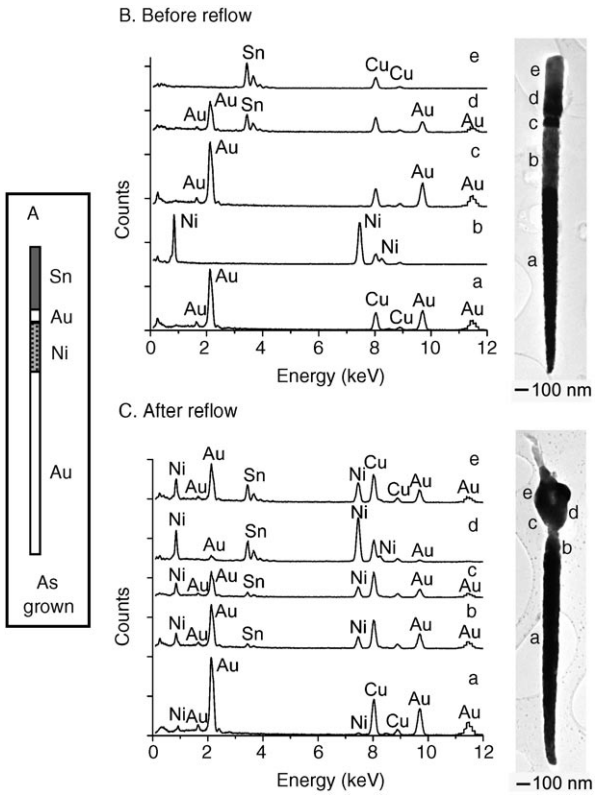

Figure 4. A) Schematic diagram of the nanowire composition of the model system studied. B, C) TEM images and energy-dispersive X-ray spectroscopy (EDS) maps taken at different points on a representative 50-nm-diameter wire, before (B) and after (C) reflow.

(≈20%).[17] After reflow (Figure 4C), we observed diffusion of Au, Ni, and Sn along the length of the wire, with a high concentration of both Ni and Au in the bulge area. This is expected because the Sn segment melts becoming a liquid, and the extent of Au and Ni dissolution in Sn is enhanced dramatically at high temperatures during reflow. We also observed that the Sn diffused into the thin Au-spacer/Ni region, which indicates good wetting of the solder on the wire. No Sn was detected in the long Au segment (Figure 4C, position a) as a result of the Ni diffusion barrier.

To characterize solder joints, we did reflow experiments with high concentrations of nanowires on substrates. We observed that solder segments on nanowires lying on top or next to each other reflowed into each other, resulting in the formation of joints. We measured the electrical resistance of nanoscale solder joints by patterning microscale contact pads on top of fused nanowires using photolithography and lift-off. The solder joints were mechanically robust enough to survive the lift-off process, which included spinning photoresist on the substrate at several thousand revolutions per minute, developing the photoresist, evaporation, and a final dissolution of the resist in acetone. The electrical resistance across the fused nanowires was measured using four probes to eliminate the contact resistance between the probes and the contact pads. We observed current–voltage (I–V) curves that were ohmic in the −0.1 to 0.1 mA region with resistances in the range of 30–200 Ω (Figure 5). Since the resistance of the actual nanowires are only a few ohms, the resistance measured across the fused nanowires is dominated by the contact resistance of the solder joint. The spread in the resistances measured can be explained by noting that the resistance of the actual solder joints depends on the overlap or the effective contact area between the solder drops on the two nanowires. In Figure 5C we have plotted a theoretical curve showing the variation of the resistance (R) per unit length (L) of Sn solder joints as a function of the effective contact radius. As we can see, the resistance of the contact depends on the overlap radius and the length of the joint. The resistance range of 30–200 Ω is significantly lower than the resistances of molecular electrical contacts measured between nanoparticles.[4] When a current of approximately 10 mA was applied between the fused wires, we lost electrical connectivity between them (open circuit). Upon analysis by SEM, we observed that the solder joint was broken at these high current densites, resulting in an open circuit.

In addition to multiple measurements of low-resistance ohmic joints between nanowires, we also observed a limited number of fused nanowires with nonlinear I–V characteristics and high resistances. We believe that these occasional higher resistance measurements are due to semiconducting and insulating oxide interfaces that occur as a result of oxi-

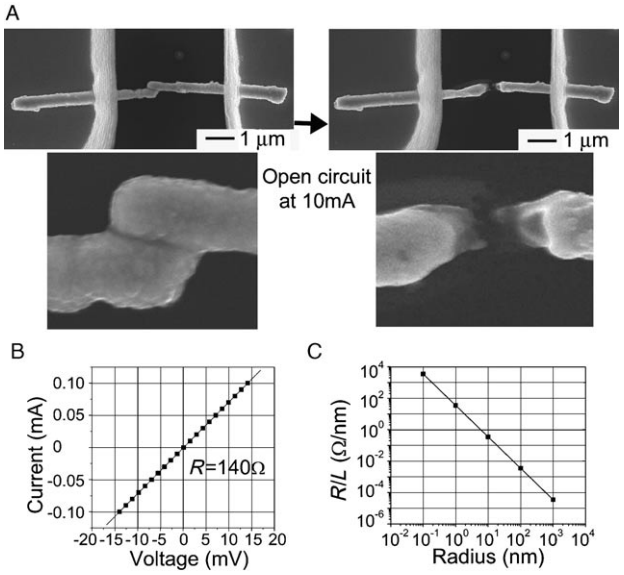

Figure 5. A) SEM images of contact pads patterned on top of fused nanowires, connected by a solder joint, before (left) electrical testing and after (right) applying a current of approximately 10 mA across the pads. The high current caused a break between the wires and resulted in an open circuit. B) A typical *I–V* curve that shows a low-resistance ohmic contact obtained across fused nanowires. C) A hypothetical curve showing the variation in resistance (*R*) per unit length (*L*) plotted against the "effective" contact radius for a metallic Sn-based joint. An electrical resistivity for Sn of 11 μΩcm was used for the calculation.

dation of the Sn segments.[18,19] Although extreme care was taken to reduce oxidation during electrodeposition, dissolution of the membrane, and reflow, the formation of thin oxide layers in some nanowire segments and solder joints cannot be ruled out. Another factor that contributed to joints with high electrical resistance was voiding that was occasionally observed at the interfaces between the different metallic segments on reflow. This voiding has been observed in prior studies of metals diffusing at interfaces and can be attributed to the Kirkendall effect.[16,20]

In conclusion, we have demonstrated that nanoparticles can be patterned with solder by electrodeposition. We have engineered a model system to investigate solder reflow down to the 30-nm length scale. This system minimizes oxidation, intermetallic diffusion, and corrosion while maintaining good wetting of solder, using a combination of a Ni diffusion barrier, a thin Au wetting layer, an organic corrosion inhibitor, and inert-N_2 gas flow during solder reflow. Oxidation, intermetallic diffusion, and corrosion greatly limit solder utility on the nanoscale by depleting the solder volume and increasing resistance of the joints. We have observed that it is possible to form low-resistance ohmic contacts between nanowires using solder. If a bottom–up strategy is pursued for the formation of electrical devices on the nanoscale, solder joints may allow for the fabrication of low-resistance electrical contacts, thereby facilitating electronic integration. We envisage the following integration scheme for the fabrication of integrated systems with electrical connectivity: a) functional nanoparticles (e.g., nanowire diodes) are patterned with solder segments; b) established self-assembly schemes, for example, magnetic assembly,[21] electrostatic assembly,[22] ligand receptor assembly,[23] and surface-tension-based assembly,[24–26] are utilized to position the particles with respect to each other and to substrates; and c) the substrates are heated to reflow the solder on the particles and form permanently bonded low-resistance interconnects, thereby forming integrated nanoelectronic devices.

Experimental Section

Fabrication of nanowires: We evaporated 200 nm of Ag (Alfa Aesar, 99.99%) in a thermal evaporator on one side of commercial alumina or polycarbonate membranes (Whatman). In the case of the polycarbonate membrane, 10 nm of chromium (Cr) was evaporated before Ag to increase the adhesion between the metal and the membrane. The membrane was placed in contact with a copper plate and restrained using a glass joint and a Viton O-ring seal. The membrane was soaked in water for 5–20 min, depending on the pore size of the membranes, and then filled with the electrolytic solution of choice. We used commercial plating solutions for Ag (Techni Silver E-2, Technic. Inc.), Au (Techni Gold 25E), Ni (Techni Nickel Sulfamate Bath RTU), Cu (Techni Copper U Bath RTU), Sn (Techni Tin), Sn/Pb (Techni Solder Matte NF820 60/40), and In (Techni Indium Sulfamate RTU). Typical electrodeposition conditions were 0.8–1.7 mA cm^{-2} for Ag, Au, Cu, and In, 10–30 mA cm^{-2} for Sn, and 30 mA cm^{-2} for Sn/Pb. The membrane was washed several times with water between each electrodeposition.

After electrodeposition, the polycarbonate membrane with the nanowires inside was dissolved in methylene chloride, and the wires were released by shaking. The wires were rinsed in methylene chloride (using sonication and centrifugation cycles) and then stored in ethanol. For alumina membranes, the Ag layer on one side of the membrane was dissolved in HNO_3 (6 M). First a drop of a solution of palmitic acid in ethanol (10 mM) was placed on the top face of the alumina membrane. Palmitic acid reacted readily with alumina, rendering the surface hydrophobic, so that nitric acid did not enter the membrane from the top face and attack the solder segments at the ends of the wires. After dissolving the Ag seed layer and rinsing several times in water, the membrane was dissolved in 0.03–0.05 M NaOH (0.1% benzotriazole (BTA) (ACROS organics) was added to the solution). Nitrogen (N_2) gas was bubbled through the NaOH solution just before dissolving the membrane to reduce the oxygen (O_2) dissolved in the solution. Mild agitation using a sonicator and a rotary evaporator was used to speed the membrane-dissolution process. After membrane dissolution was complete, the NaOH was removed by centrifugation at 5000–6000 rpm for 5–6 min, and the wires were rinsed repeatedly with water and ethanol and then stored in ethanol.

Solder reflow: A suspension of nanowires in ethanol was sonicated (for 10–20 s) before deposition to disperse the wires. A few drops of the solution were placed on a silicon (SiO_2-coated) substrate and the ethanol was allowed to evaporate. The reflow was carried out in a tube furnace that was sealed and purged with N_2 (30 kPa) before, during, and after reflow to pre-

vent oxidation of the nanowires and solder joints that formed. We used a Pyrex tube in the furnace for reflow. All the glass joints were sealed using Apiezon high-temperature grease to minimize any oxygen leakage. The temperature in the tube was calibrated against the furnace temperature using a thermocouple. The temperature was first increased to approximately 180 °C for 3 min to preheat the wires, it was then raised briefly to 300 °C to ensure complete reflow. The tube was then brought out of the furnace and cooled down to room temperature. We arrived at the optimum reflow temperature profile after repeated experiments with different temperature conditions. SEM images were taken on a JEOL JSM-6700F field-emission scanning electron microscope at 10 kV. TEM images were taken with a Philips CM300 FEG operating at 297 kV.

Fabrication of contact pads: To pattern microscale contact pads, a layer of photoresist (Shipley 1813) was spun on the substrate, and a contact-pad mask was aligned with the wires held together by a joint. After developing the photoresist, a thin film consisting of 50 nm of Cr and 350 nm of Cu was evaporated on the substrate, and the photoresist was dissolved in acetone.

Electrical measurements of solder joints between nanowires: The resistance of fused nanowires was measured using a four-terminal measurement across the two contact pads. The outer two pairs of probes carried current, and the inner two pairs were used to measure the voltage across the wires. This method eliminates the resistance of the contact between the probes and the pads from the measurement results. Since we used a four-probe measurement across two contact pads (as opposed to four contact pads as is done in a traditional four-point probe measurement), the contact resistance between the contact pads and the nanowires under them remain included in the total resistance measured. This resistance between the contact pads with nanowires underneath is of the order of 1–2 Ω (we have measured this value experimentally in control samples), which is negligible compared to the total resistance of fused nanowires measured (30–200 Ω). The *I*–*V* curves were obtained using a Keithley 2400 digital source meter by scanning the current from −0.1 to 0.1 mA.

Keywords:

interconnects · nanoelectronics · nanotechnology · nanowires · solder reflow

[1] J. S. Hwang, *Modern Solder Technology for Competitive Electronics Manufacturing*, Electronic Packaging and Interconnection Series, McGraw-Hill, New York, **1996**.
[2] J. H. Lau, *Ball Grid Array Technology*, McGraw-Hill, New York, **1994**.
[3] C. H. Jan, N. Anand, C. Allen, J. Bielefeld, M. Buehler, V. Chikamane, K. Fischer, K. Jain, J. Jeong, S. Klopcic, T. Marieb, B. Miner, P. Nguyen, A. Schmitz, M. Nashner, T. Scherban, B. Schroeder, C. Ward, R. Wu, K. Zawadzki, S. Thompson, M. Bohr, in *Proc. 7th IEEE Int. Interconnect Technol. Conf.*, San Francisco, CA, June 7 – 9, 2004, p. 205.
[4] X. D. Cui, A. Primak, X. Zarate, J. Tomfohr, O. F. Sankey, A. L. Moore, T. A. Moore, D. Gust, G. Harris, S. M. Lindsay, *Science* **2001**, *294*, 571.
[5] K. F. Harsh, V. M. Bright, Y. C. Lee, in *Proc. Electron. Compon. Technol. Conf.*, Las Vegas, NV, May 21 – 24, 2000, p. 1690.
[6] F. Banhart, *Nano Lett.* **2001**, *1*, 329.
[7] H. Ye, Z. Gu, T. Yu, D. H. Gracias, *IEEE Trans. Nanotech.*, in press.
[8] C. R. Martin, *Chem. Mater.* **1996**, *8*, 1739.
[9] B. R. Martin, D. J. Dermody, B. D. Reiss, M. Fang, L. A. Lyon, M. J. Natan, T. E. Mallouk, *Adv. Mater.* **1999**, *11*, 1021.
[10] H. H. Manko, *Solders and Soldering*, 4th ed., McGraw-Hill, New York, **2001**, pp. 135 – 143.
[11] Y. Li, K.-S. Moon, C. P. Wong, *Science* **2005**, *308*, 1419.
[12] Y. S. Tan, M. P. Srinivasan, S. O. Pehkonen, S. Y. M. Chooi, *J. Vac. Sci. Technol. A* **2004**, *22*, 1917.
[13] B. F. Dyson, *J. Appl. Phys.* **1966**, *37*, 2375.
[14] L. Buene, H. Falkenberg-Arell, J. Gjønnes, J. Taftø, *Thin Solid Films* **1980**, *67*, 95.
[15] D. Gregersen, L. Buene, T. Finstad, O. Lønsjø, T. Olsen, *Thin Solid Films* **1981**, *78*, 95.
[16] J.-G. Wang, M.-L. Tian, T. E. Mallouk, H. W. M. Chan, *Nano Lett.* **2004**, *4*, 1313.
[17] S. Varghese, C. I. Muneera, V. Unnikrishnan Nayar, *Thin Solid Films* **1983**, *99*, 385.
[18] Z. Liu, D. Zhang, S. Han, C. Li, T. Tang, W. Jin, X. Liu, B. Lei, C. Zhou, *Adv. Mater.* **2003**, *15*, 1754.
[19] P. M. Gorley, V. V. Khomyak, S. V. Bilichuk, I. G. Orletsky, P. P. Horley, V. O. Grechko, *Mater. Sci. Eng. B* **2005**, *118*, 160.
[20] Y. Yin, R. M. Rioux, C. K. Erdonmez, S. Hughes, G. A. Somorjai, A. P. Alivisatos, *Science* **2004**, *304*, 711.
[21] C. J. Love, A. R. Urbach, M. G. Prentiss, G. M. Whitesides, *J. Am. Chem. Soc.* **2003**, *125*, 12696.
[22] H. O. Jacobs, S. A. Campbell, M. G. Steward, *Adv. Mater.* **2002**, *14*, 1553.
[23] W. Shenton, S. A. Davis, S. Mann, *Adv. Mater.* **1999**, *11*, 449.
[24] Z. Gu, Y. Chen, D. H. Gracias, *Langmuir* **2004**, *20*, 11308.
[25] D. H. Gracias, J. Tien, T. L. Breen, C. Hsu, G. M. Whitesides, *Science* **2000**, *289*, 1170.
[26] H. O. Jacobs, A. R. Tao, A. Schwartz, D. H. Gracias, G. M. Whitesides, *Science* **2002**, *296*, 323.

Received: August 19, 2005

